Accepted Manuscript

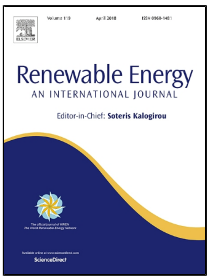

Comparison of different CSP technologies for combined power and cooling production

S. Ravelli, G. Franchini, A. Perdichizzi

PII:	S0960-1481(18)30084-3
DOI:	10.1016/j.renene.2018.01.074
Reference:	RENE 9679
To appear in:	*Renewable Energy*
Received Date:	20 September 2017
Revised Date:	20 December 2017
Accepted Date:	19 January 2018

Please cite this article as: S. Ravelli, G. Franchini, A. Perdichizzi, Comparison of different CSP technologies for combined power and cooling production, *Renewable Energy* (2018), doi: 10.1016/j.renene.2018.01.074

This is a PDF file of an unedited manuscript that has been accepted for publication. As a service to our customers we are providing this early version of the manuscript. The manuscript will undergo copyediting, typesetting, and review of the resulting proof before it is published in its final form. Please note that during the production process errors may be discovered which could affect the content, and all legal disclaimers that apply to the journal pertain.

ACCEPTED MANUSCRIPT

Comparison of different CSP technologies for combined power and cooling production

S. Ravelli, G. Franchini*, A. Perdichizzi

Department of Engineering and Applied Sciences, University of Bergamo, 5 Marconi Street, Dalmine 24044, Italy

Abstract

The present paper deals with the performance prediction of Concentrated Solar Power plants integrated with cooling energy production. The plant configuration is based on a typical steam Rankine cycle (rated 62.1 MW_e). The thermal input is provided by two different solar fields: i) Parabolic Trough Collectors and ii) Central Receiver System with heliostats reflecting on the tower top. In the former case, both north-south and east-west oriented collectors are investigated and compared in the study. A Thermal Energy Storage system allows driving the power block 24-hour per day also in periods with low solar irradiation. A steam flow rate extracted from the turbine low stages feeds a set of two-stage absorption chillers, and the produced chilled water is supplied to a district cooling network. A computer code integrating the commercial software Thermoflex and Trnsys has been developed to model and to simulate over 1-year period the solar field and the power block.

The power plant is supposed to operate in island mode, having to meet power and cooling demand for a population of about 50,000 inhabitants in the Saudi desert region. Solar fields and storage system were sized according to a techno-economic optimization algorithm for the minimization of the investment costs. The simulation results show the beneficial effect of the combined power and cooling production in terms of peak load shaving. Compared to the troughs, solar tower exhibits a higher efficiency, thus requiring a lower aperture area and lower investment costs. The techno-economic analysis shows that the axis orientation has a strong impact on the trough collectors and that east-west oriented devices perform better for the investigated load-following application.

Keywords: Absorption Chiller; Central Receiver System; Combined Cooling and Power; Concentrating Solar Power; Parabolic Trough; Steam Rankine Cycle.

Nomenclature

Aa	aperture area (m^2)
ABS	absorption chiller
C_a	cost per unit area (USD/m^2)

* Corresponding author. Tel.: +39 035 2052078; fax: +39 035 2052077.
E-mail address: giuseppe.franchini@unibg.it.

ACCEPTED MANUSCRIPT

C_v	cost per unit volume (USD/m^3)
CCHP	combined cooling heating power
COP	coefficient of performance
CRS	central receiver system
CSP	concentrated solar power
E_{coll}	collected heat (MWh)
E_d	energy deficit (MWh)
E_{dem}	heat demand (MWh)
E_{rad}	incident solar energy (MWh)
EC	economizer
EV	evaporator
DNI	direct normal irradiation (W/m^2)
HTF	heat transfer fluid
HX	heat exchanger
I_b	beam radiation (W/m^2)
K	incident angle modifier
LCOE	levelized cost of electricity (USD/kWh)
LP	low pressure
MED	multi-effect distillation
p	penalty factor (USD/MWh)
p_{cond}	condenser pressure (bar)
P_{chill}	electric chiller power consumption (MW)
P_{dem}	power demand (MW)
P_{res}	residual power demand (MW)
PTC	parabolic trough collector
PV	photovoltaics
Q_{abs}	absorption chiller cooling power (MW)
Q_{coll}	collected thermal power (MW)
Q_{cool}	cooling demand (MW)
Q_{dem}	thermal power demand (MW)
Q_{rad}	incident solar radiation (MW)
RH	re-heat
SH	super-heater
T_{amb}	ambient temperature (K)
T_{av}	average temperature (K)
T_{sky}	sky temperature (K)
TES	thermal energy storage
V_t	tank volume (m^3)
V_{wind}	wind speed (m/s)

ACCEPTED MANUSCRIPT

ACCEPTED MANUSCRIPT

73	ε	emissivity (-)
74	η_{opt}	optical efficiency (-)
75	η_{PTC}	parabolic trough overall efficiency (-)

76

1. Introduction

78 The interest in CSP technologies has been growing over the past ten years. A number of new plants have
79 been brought on line since 2006 as a result of declining investment costs and LCOE, as well as new support
80 policies. Nevertheless, CSP must compete against PV technology, which is undergoing large price reductions
81 over the last few years [1]. The debate of whether CSP or PV power plants will prevail is topical. Besides
82 pricing, CSP faces other challenges like inability to exploit diffuse radiation, criticisms related to heat
83 rejection and water consumption (in water-driven heat rejection systems), and long lead-time for plant
84 construction.

85 However, a key benefit of CSP over PV is that CSP plants can more easily provide ancillary services and
86 provide dispatchable power on-demand using long-term storage [2,3]. This point makes CSP plant highly
87 flexible and ideal especially for remote locations, where electric power must be imported via expensive
88 transmission infrastructures. According with IEA report [4], off-grid or remote-grid CSP systems comprise
89 around 10% of the overall CSP capacity.

90 Beyond electricity generation for remote or weakly interconnected grids, CSP plants can provide process
91 heat for final uses or for feeding thermally driven chillers (CCHP). In a Rankine cycle power plant, a steam
92 flow rate can be extracted from the low-pressure steam turbine and be supplied to absorption chillers; the
93 generated chilled water is then delivered to a district cooling system. This option allows replacing
94 conventional electric chillers leading to a significant peak power reduction on the grid and a general
95 flattening of the electric load pattern [5]. This is a way to increase virtually the solar-to-electric efficiency of
96 CSP plants (because the power demand on the grid decreases and this is equivalent to a power extra-
97 production), thus improving their competitiveness.

98 Worldwide, many electric companies faced rapid growth in electricity demand peaks in the last years. The
99 main reason is a rise in the use of air conditioning units. Absorption chillers, by shifting cooling from an
100 electric to a thermal load, are able to reduce demand charges throughout the year and summer peak loads.
101 Moreover, despite a lower coefficient of performance (COP) as compared to mechanical chillers, they can
102 substantially reduce operating costs because they are fed by low-grade waste heat [6]. In the open literature,
103 some papers focus on the investigation of solar driven CCHP systems, but most of them deal with small-
104 scale engines [7,8].

105 The integration of desalination systems in CSP plants is another way to increase the overall efficiency. In
106 particular, thermal desalination techniques permit to reuse the low-grade energy released to the atmosphere.
107 The combination of multi-effect distillation (MED) with concentrated solar power plants is considered one
108 the most promising options, for a combined freshwater and power production in CSP plants close to the sea
109 [9,10].

110 The purpose of this study is to demonstrate that a solar-driven Rankine cycle with a thermal storage can

ACCEPTED MANUSCRIPT

be flexibly operated to match both electric and cooling demand over a one-year period. Four CSP technologies are on the market: parabolic troughs, linear Fresnel reflectors, solar towers and dish/engine systems. Among these options, parabolic troughs and more recently towers have been installed in commercially operating plants [11]. The most used plant configuration involves indirect steam generation by means of a thermal fluid circulating in the solar field. Conventional HTFs used in solar power plants are synthetic oil and molten salt. The former is by far the most common solution in spite of temperature limitation (about 400°C) as well as flammability and toxicity features. The latter can reach much higher temperatures (over 600°C), allowing for steam temperature increase up to 550°C, with a significant benefit for the steam cycle efficiency. Moreover, molten salt is less expensive and more environmentally benign than the other HTFs. The main drawback of molten salt is the high freezing point (about 250°C), together with the requirement of stainless steel materials because of corrosion issues. A third solution is Direct Steam Generation (DSG): water evaporates and the resulting steam is superheated in the solar loop without needing a heat exchanger between solar field and power block. DSG technology has been experimentally investigated for years and is now operating commercially (PS10 and PS20 tower plants in Seville, Puerto Errado 2 Fresnel plant in Murcia region, TSE-1 PTC plant in Thailand, Khi Solar One in South Africa, Ivanpah project in California) [12].

The thermal energy storage (TES) plays an important role in improving the performance and reliability of solar thermal power plants. It allows to mitigate the effects of fluctuations in solar intensity and to extend (or to shift) the operation of the plant. Thus, the plant can operate much more flexibly and the mismatch between the power generated by the Sun and the electricity demand profile can be reduced. The most common TES solution for solar thermal power plants is a two-tank storage system. The indirect system uses different fluids as storage medium (molten salt) and HTF (thermal oil), whilst in the CSP plants with direct storage the HTF (molten salt) also serves as storage medium. This concept (with higher cost savings) was successfully demonstrated both in PTC plant (13.8 MW_e SEGS I plant; 120 MWh_t storage capacity) and tower plant (10 MW_e Solar Two; 105 MWh_t storage capacity) [13].

Despite a large number of studies investigating single CSP technologies, only a few works make a comparison between different solar fields based on PTCs and CRS, respectively. Solar collector efficiency is strongly related to site latitude and meteorological conditions (DNI, ambient temperature) [14]. Generally speaking, PTCs can collect a larger amount of incident radiation in summer months than heliostats with identical aperture area, but their efficiency tends to dramatically decay in winter [15]. Comparing the results from parabolic trough and tower plants, the latter typically provide a higher uniformity in the electricity production, due to a more constant thermal collection capability all over the year. However, because of the larger spacing needed by the heliostats, the energy density is lower than for the PTC plants [16]. Furthermore, PTC axis orientation can affect the energy delivery. In fact, the thermal energy collected by a solar field with troughs whose axis is north-south oriented may vary a lot during the year. Conversely, the thermal energy delivered by PTCs with east-west axis orientation does not vary so much from summer to winter. Nevertheless, the yearly thermal output of a PTC with tracking axis oriented north-south is greater [17,18]. This is why current solar thermal power plants operating with a maximum-load logic all use north-south oriented collectors [19].

ACCEPTED MANUSCRIPT

In a previous preliminary work [20], the authors demonstrated that the integration of CSP plants and cooling production is beneficial to increase the global efficiency. Starting from that concept of combined cooling and power plant, the authors developed an all-new modeling procedure for simulating parabolic troughs and solar towers, including the thermal energy storage management for a load following strategy. Moreover, in the present paper a multi-variable optimization procedure has been developed to determine the optimal size for each solar field (aperture area) and for the storage system (hot and cold tank volume). The present investigation aims to explore and compare the performance of a fully solar-driven plant for three different CSP solutions: i) PTCs with north-south axis orientation, ii) PTCs with east-west axis orientation, and iii) CRS. The paper presents also an economic sensitivity analysis, aiming to discussing the impact of the budget costs on the simulation results.

2. Design conditions and assumptions

The modeling assumptions are reported in this section, for both the CSP plant configurations (PTC and CRS). Attention is focused separately to the power block (including absorption chillers) and the solar field.

2.1 Electric and cooling load

The power system is assumed to operate in island mode and it was sized for a community of about 50,000 inhabitants. Daily patterns of power and cooling demand were derived from data supplied by power utilities operating in the Gulf area and are defined for a one-year period. Figure 1 shows the total power load (yellow) and the fraction of power consumption due to chillers (cyan) for a typical summer and winter day. The power demand undergoes large variations between summer and winter, and between day and night hours. The power needs for electric chillers range from 15% in winter to 45% of the total demand in summer. A detailed description of the considered electric and cooling load is given in [5].

The combined power and cooling production into a CSP plant produces as effect a more flattened power load. Absorption chillers allow displacing a portion of the cooling load, making possible a significant reduction of the power demand, especially in the hours with the highest cooling request. Moreover, a correctly sized thermal storage permits to reduce the aperture area of the solar collector field and to avoid the use of back-up systems.

ACCEPTED MANUSCRIPT

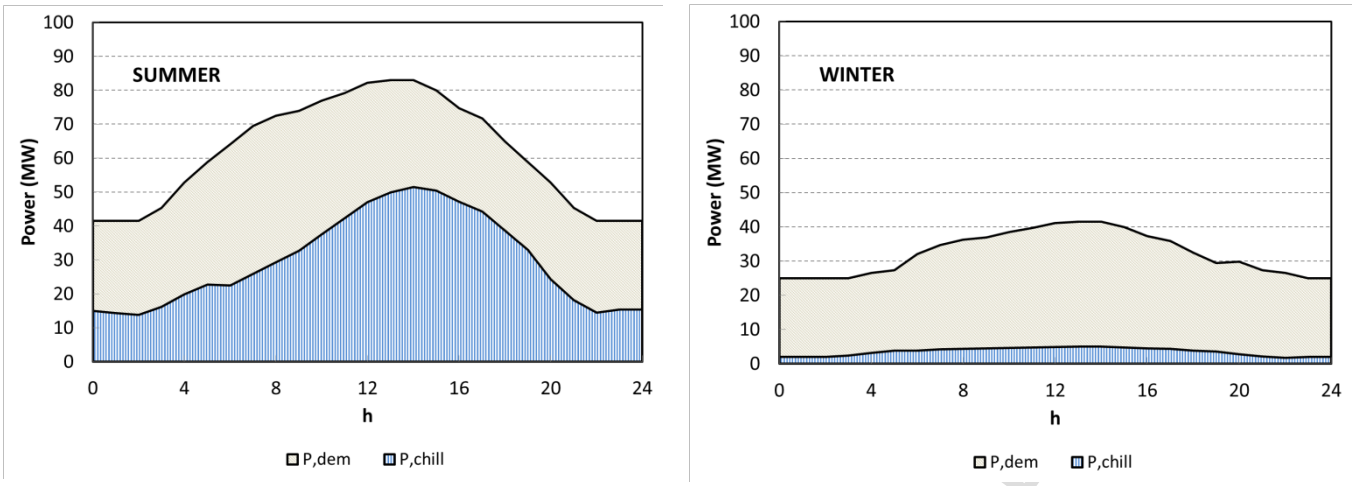

Fig. 1. Electric load (P_{dem}) and chiller power consumption (P_{chill}).

2.2. *Power block*

Figure 2 shows the power plant configuration. It is the typical scheme of a steam Rankine cycle, with air condenser, a set of feed-water heaters and a deaerator. A fraction of the steam flow rate is extracted upstream of the LP turbine to drive four double-stage absorption chillers, each one with nominal cooling capacity 20.7 MW and COP 1.31. The chilled water is supposed to be supplied to a district cooling system. The solar heat is the only thermal input: no auxiliary heaters are considered. A detailed description of the power block is presented in [20]. Primary thermal design parameters are from [21], whilst Table 1 summarizes the design conditions.

Thanks to the cooling energy provided by the absorption chillers, the electricity requirement is significantly lowered, as documented in the paragraph 4 "*Simulation results*". The power output (62.1 MW at design conditions) is high enough to meet the power demand on the electrical grid.

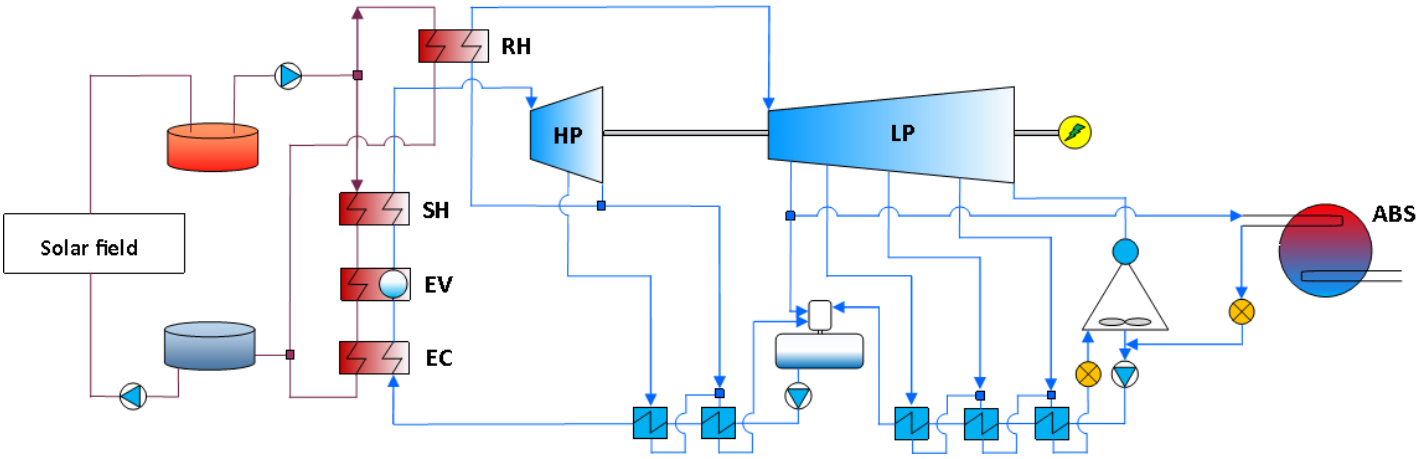

Fig. 2. Schematic of the investigated CSP plant.

ACCEPTED MANUSCRIPT

Table 1

Rankine Cycle parameters at ISO conditions.

Turbine inlet temperature (°C)	540
Turbine inlet pressure (bar)	100
Steam mass flow at turbine inlet (kg/s)	67.6
Reheat temperature (°C)	500
Average turbine efficiency (%)	86
Extraction pressure (bar)	8
Condenser pressure (bar)	0.06
SH+EV+EC thermal power (MW)	167.0
RH thermal power (MW)	24.9
Net electric power (MW)	62.1
Thermal efficiency (%)	32.3

2.3. Solar field

PTC and CRS have been considered as solar fields. With regard to the PTC axis alignment, it is well known that the north-south orientation allows for a higher solar energy collection on annual basis; nevertheless, for this investigation the east-west orientation has been considered as well because it can be suitable for the load-following strategy of the present case study. For each solar configuration, a two-tank molten salt direct storage system is implemented in the modeling [22]. HTF (molten salt mixture, 60% $NaNO_3$ 40% KNO_3) coming from solar field fills the hot tank; then it is withdrawn to transfer heat to the steam generator. A cold tank finally collects molten salt exiting heat exchangers and acts as a buffer. It has to be reminded that the CSP plant is designed to operate in *island mode*; hence, TES and solar field must cover hour by hour the heat demand of the Rankine cycle.

3. Methods and tools

The simulations have been carried out according to Meteonorm climate data related to Riyadh (Saudi Arabia). Figure 3 shows ambient temperature and DNI for a typical day in summer and a typical day in winter. It has to be pointed out that the daily profiles of solar radiation are not theoretically calculated according to Sun position, but are measured including cloud, pollution and dust effects. The annual DNI amounts to 2 337 kWh/m^2.

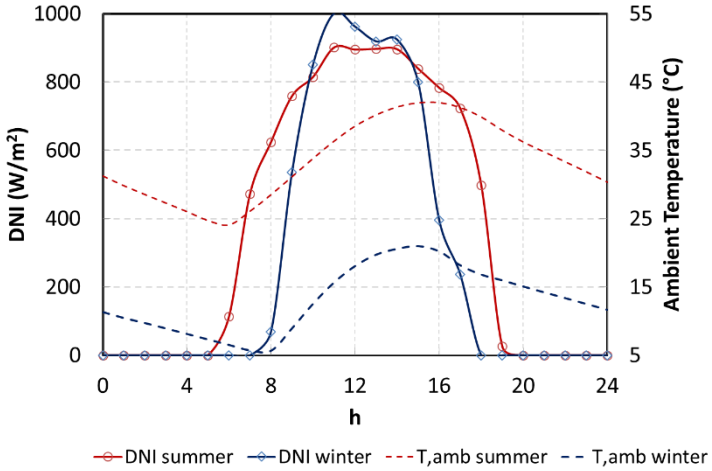

Fig. 3. Meteorological conditions.

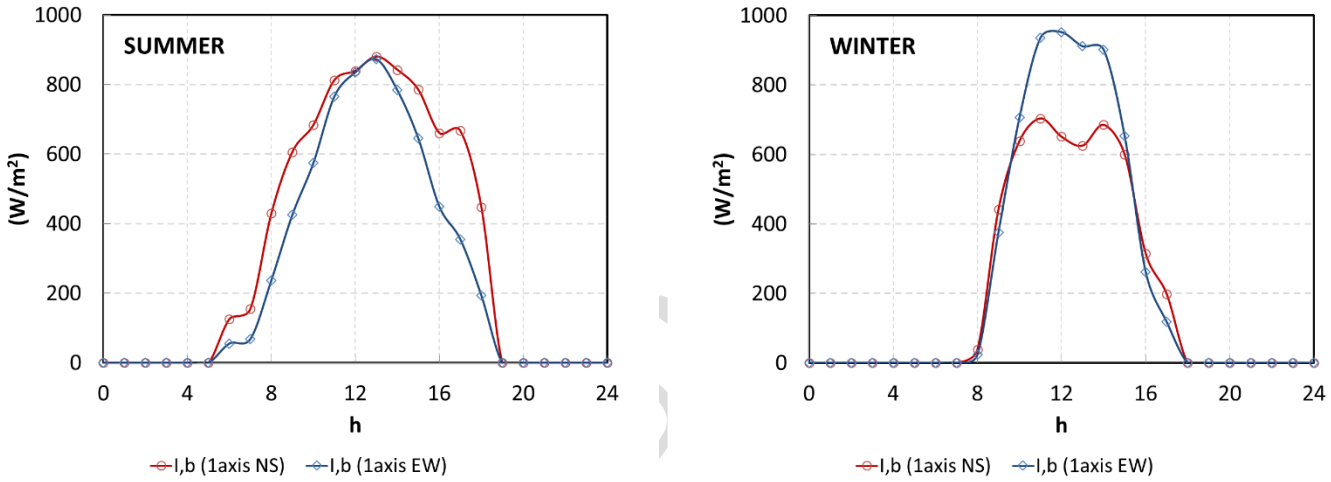

Fig. 4. Beam radiation captured by 1-axis tracking systems.

With regard to the influence of the PTC axis orientation on the incident beam radiation, Figure 4 shows the direct solar irradiance that 1-axis tracking systems north-south and east-west oriented can capture for the two representative days. In summer, the north-south orientation allows for collecting a larger amount of beam radiation, mainly when the solar azimuth angle is high (in the morning and in the afternoon). On the contrary, the east-west oriented solar devices, tracking the Sun along its altitude, can intercept a significantly higher solar radiation in the central hours of a winter day.

The simulations were carried out for a one-year period on hourly basis. With regard to the computer model, firstly it has to be underlined that in every modeling activity the selection of the level of investigation is a crucial point. The present work targeted a compromise between a detailed analysis and an evaluation of the overall performance. Thermoflex® has been used to simulate the power block, whilst the solar fields and the absorption chillers were modeled and simulated in Trnsys® environment, including TESS® libraries. The PTC solar field consists in a number of loops depending on the required total aperture area. Each loop has 8 solar collector assemblies (SCA) with total length per SCA 115 m. The trough overall efficiency under actual

ACCEPTED MANUSCRIPT

operating conditions was evaluated as follows:

$$\eta_{PTC} = \eta_{opt} \cdot K - \left(A + C \cdot V_{wind}\right) \cdot \frac{\left(T_{av} - T_{amb}\right)}{I_b} - \varepsilon \cdot B \cdot \frac{\left(T_{av}^4 - T_{sky}^4\right)}{I_b} \quad (1)$$

where T_{av}, T_{amb} and T_{sky} are the HTF average temperature, the dry-bulb ambient temperature and the effective sky temperature for long wave radiation calculations, respectively, V_{wind} is the wind speed, ε is the absorber emissivity and I_b is the direct solar irradiance. The coefficients A, B and C were computed to fit the thermal efficiency curve of Schott PTR70 receivers under standard conditions [23]. The optical efficiency η_{opt} (0.77) takes into account mirror reflectivity, glass transmissivity and receiver tube absorptivity. The incident angle modifier K is related to the effect of the non-perpendicularity of solar radiation and it is a function of the incidence angle.

Trnsys® was also used to model the heliostat solar field (120 m^2 heliostat surface) and the tower receiver. Several codes based on ray-tracing software are available in the literature for the design and the optimization of the heliostat layout [24,25]. Most of them focus on the analysis of the single mirror performance, whilst the level of investigation of the present work requires an overall efficiency of the solar field under variable operating conditions. So, the heliostat field performance was evaluated by means of an efficiency map derived from the System Advisor Model (SAM) developed by the National Renewable Energy laboratory (NREL) [26]. In detail, SAM was preliminary used to generate optimized heliostat layouts for power plant ranging from 5 to 200 MW$_e$ under Riyadh climate conditions. For each size and for each azimuth and altitude combination a field efficiency has been calculated. The resulting efficiency map is shown in graphical way in Fig. 5. The overall heliostat field efficiency (including mirror reflectivity, cosine loss, spillage and atmospheric attenuation) is dependent on the plant size (affecting the heliostat layout and the tower height) and on the solar zenith angle, whilst the azimuth angle has a minor impact on the field efficiency. The solar receiver at the tower top was simulated as a simple black body absorber, with thermal losses computed on a receiver area of 25 m^2.

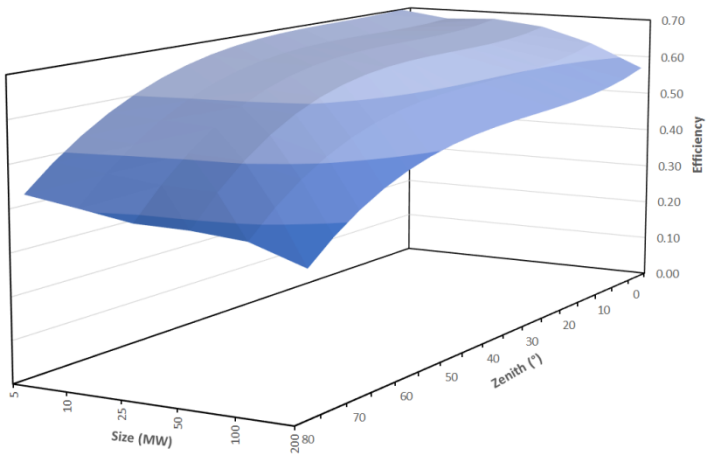

Fig. 5. Efficiency map of the heliostat field.

ACCEPTED MANUSCRIPT

Moving to the simulation algorithm, firstly an iterative procedure within Thermoflex® provides hour-by-hour the HTF flow rates ensuring that the Rankine cycle power output equals the current requirement on the electrical grid. The power block is simulated to match both power and cooling demand all the time, coherently with the island operation mode. Then, Trnsys® takes the computed HTF flow rates as input for the solar field and the TES system. PTCs and CRS provide the required molten salt flow rate just to feed the power cycle through the heat exchangers HX1 and HX2.

Concerning the power block, it has to be pointed out that the steam turbine is called to operate most of the time in off-design conditions. The steam flow rate at turbine outlet may differ significantly from design condition since LP turbine flow is always adjusted to match both electrical and cooling demands. Therefore the turbine Thermoflex® model included both admission control valves and exhaust losses to simulate the turbine off-design behavior accurately.

The off-design operation of absorption chillers has been considered according to the performance maps provided by the manufacturers. Figure 6 shows the cooling capacity and the heat input (both are indicated as percentage of the nominal cooling capacity) and the coefficient of performance for the considered two-stage lithium-bromide absorption chiller at partial load.

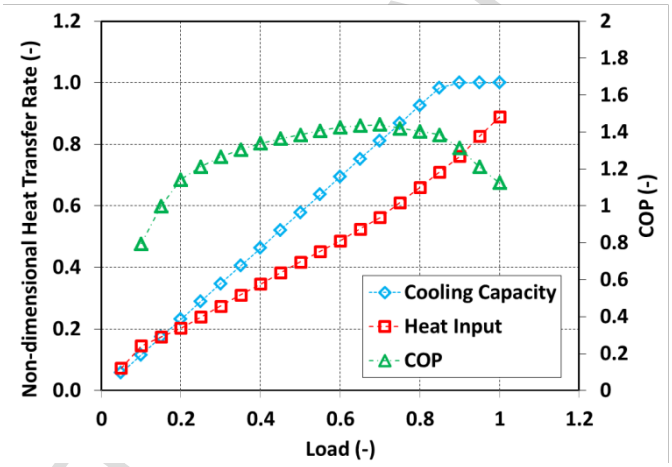

Fig. 6. Two-stage absorption chiller performance map [5].

To select the right size of solar field and storage tanks, an optimization procedure interacting with Trnsys® model and based on GenOpt® tool [27] was used. Figure 7 shows the interaction of the simulation tools. As mentioned before, firstly Thermoflex® evaluates hour-by-hour the heat input demand to meet both power and cooling demand. Then, Trnsys® simulates the solar field including TES system, which supplies the required HTF flow rate. The storage system charges and discharges according to the HTF flow rate required by the power block. GenOpt® interacts with Trnsys® by replacing the values of the decision variables according to the Hooke-Jeeves pattern search algorithm. Table 3 reports the optimization variables, the range within which they are optimized, the initial step size, and the starting point.

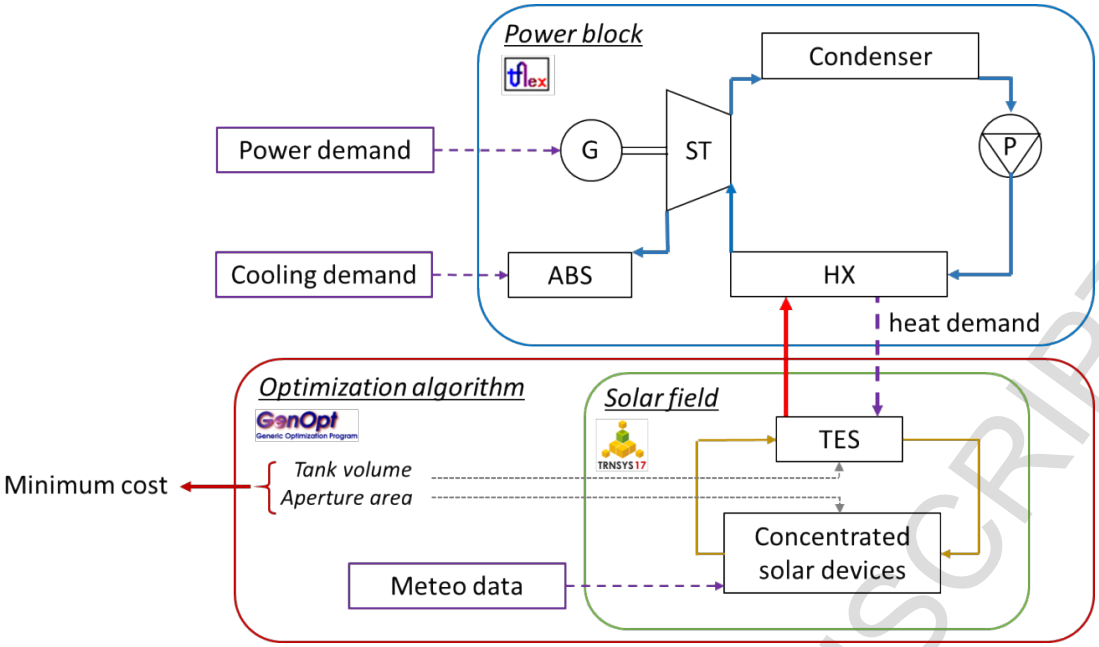

Fig. 7. Optimization algorithm.

Table 3
Optimization Variables

	Range	Initial step size	Initial value
Aperture area (m^2)	800,000-2,500,000	100,000	1,500,000
Tank volume (m^3)	20,000-60,000	10,000	40,000

On the base of annual Trnsys® simulations, GenOpt® determines the optimal values for aperture area and storage tank volume, minimizing the budget cost. The budget cost (C) is a cost estimation limited to the solar devices and the storage system; it is calculated starting from the cost per unit of aperture area for PTC and CRS respectively, and the cost per unit of stored energy for the TES system reported in Table 4. The authors are aware that the costs of CSP components undergo rapid variations depending on the technology development. For this investigation, the values reported in Table 4 were derived from [26] and [28] as representative of current investment costs. Nevertheless, in the last paragraph a sensitivity analysis on the budget costs will be presented, in order to extend the paper results to other different economic scenarios.

Table 4
Budget costs

	PTC	CRS
C_a (USD/m^2)	250	300
C_v (USD/kWh)	30	30

The optimization objective function (C) is calculated as follows:

ACCEPTED MANUSCRIPT

ACCEPTED MANUSCRIPT

$$C = C_a \times A_a + C_v \times V_t + p \times E_d \quad (2)$$

where p is a penalty factor (10^{15} USD/MWh) and E_d is the annual thermal energy deficit occurring whenever the hot storage tank is empty. The last term in the equation permits to neglect all solutions that do not respect the constraint of meeting power and cooling demand without fossil backup.

4. Simulation results

Firstly, the results of the optimization procedure are shown. Table 5 indicates the optimal values of aperture area and tank volume computed by GenOpt® for the three investigated solar configurations. It is worth highlighting that for the considered power and cooling demand CRS technology requires a significantly lower aperture area than PTCs (-38%), and that east-west orientation allows to reduce the required trough surface (-5%), although the yearly solar radiation collected by a PTC north-south oriented is higher. These results are consistent with the seasonal performance discussed in the next sections. Likewise, north-south oriented PTCs need a higher storage capacity (+35%), due to the high performance variation between summer and winter, as documented later on.

Table 5
Optimal design parameters

	PTC $_{\text{north-south}}$	PTC $_{\text{east-west}}$	CRS
A_a (m^2)	1,815,000	1,722,800	1,041,360
V_t (m^3)	49,800	37,000	35,600

4.1. Daily simulation results

The simulation of the CSP plants has been performed over a one-year period to evaluate the annual yield. First, results will focus on two representative summer and winter days. Then, monthly and annual simulation outputs will be presented to discuss potential and limitations of the investigated solar fields.

Figure 8 shows the cooling demand (gray) and the cooling energy provided by the absorption chillers (light blue) for the two selected days. In summer, the absorption chillers cannot meet the peak demand: backup electric chillers (rated 50 MW cooling capacity) are supposed to fill the gap. Nevertheless, the number of operating hours for these units covering the peaks is very low. The *COP* of electric chillers is considered variable with ambient temperature in the range between 2.5 (at T_{amb} = 42°C) and 5 (at T_{amb} = 24°C). During the winter day, when the cooling demand is low, a limited steam flow rate is extracted to drive the absorption chillers, leaving the remaining flow rate expanding in the LP turbine section.

ACCEPTED MANUSCRIPT

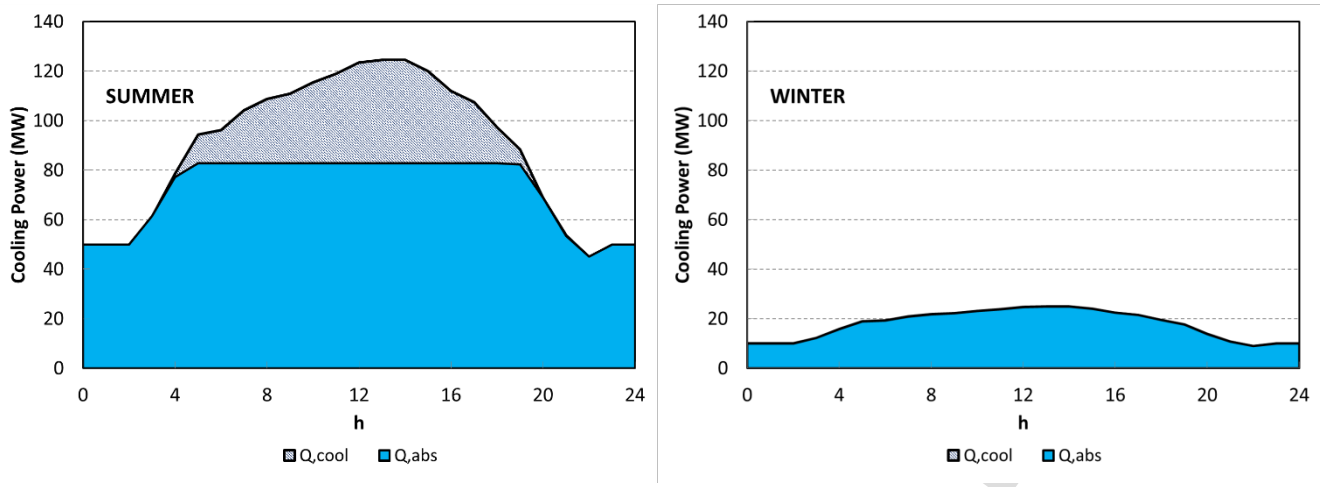

Fig. 8. Cooling load curves.

The impact on the electrical grid due to the chilled energy supplied by absorption chillers via district cooling network is shown in Fig. 9. The original power demand (light area) is lowered down to the residual electric demand, P_{res}. The energy savings is in the range 10-30 MW_e in summer and 2-5 MW_e in winter, according to the cooling demand curves previously discussed.

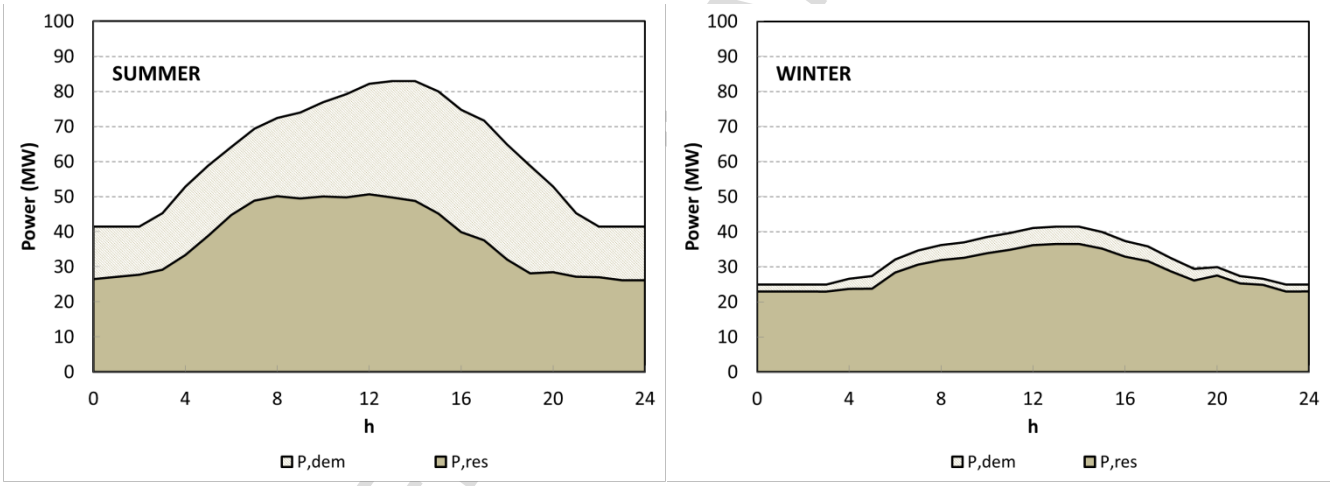

Fig. 9. Power demand in the scenario of integrated district cooling.

Hour by hour, the CSP plant adjusts the total steam flow rate and the steam extraction in order to meet the current power demand, P_{res}, and the cooling demand, Q_{abs}. The adjustment of the steam flow rate and the ambient temperature variation affect also the condenser performance. The pressure level in the condenser varies as shown in Fig. 10; when ambient temperature approaches 45°C, the air-cooled condenser operates at 0.23 bar, whilst steam condensation takes place close to 0.05 bar in the winter day. This is a combined effect of the cold temperatures and the low steam flow rate at part load.

In winter, the cycle efficiency, evaluated as the ratio of the net power output to the solar heat, approaches 35% thanks to the low ambient temperatures. On the contrary, hot temperatures in summer penalize the air condenser performance, leading to an efficiency in the range between 28% and 23%. The steam extraction

ACCEPTED MANUSCRIPT

for driving the absorption chillers produces a further performance penalty when the cooling demand is high.

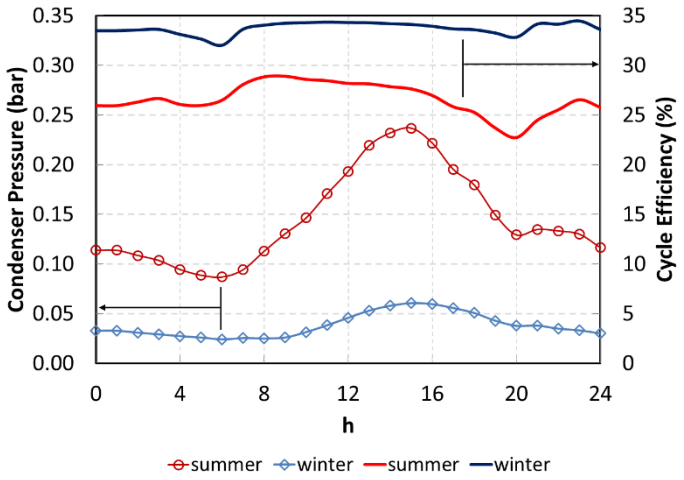

Fig. 10. Condenser pressure and cycle efficiency.

With regard to the solar field performance, Figs. 11, 12 and 13 show the results for the parabolic trough cases north-south and east-west oriented, and the solar tower case, respectively. Every plot reports the solar radiation entering the aperture area (Q_{rad}), the collected heat (Q_{coll}), the heat delivered to the power block (Q_{dem}) and the filling level of the hot storage tank. The PTC configuration with a north-south orientation (Fig. 11) undergoes a strong variation in the collector efficiency between summer and winter: the peak Q_{coll} in winter is roughly half that in summer (500 MW vs. 1050 MW). In the daytime, the collected heat exceeds the heat requirement of the power plant. The surplus allows charging the hot storage tank. In summer when the tank is full (from 10^h to 18^h), a number of troughs must be defocused [29], whilst in the winter day the daily heat surplus is negligible.

With east-west axis orientation (Fig.12), the peak Q_{coll} in winter is about 72% of that in summer, corresponding to moderate variations between warm and cold seasons. Moreover, the need of defocusing is much lower, as documented by the shorter period with full storage tank in the summer day (from 12^h to 17^h). For a given season, the comparison between the collected heat profiles with different axis orientation shows that the thermal output from the north-south collectors is higher in summer (+53%), whereas in winter the daily thermal outputs are similar (3130 MWh/day vs. 3630 MWh/day). Nevertheless, the east-west oriented configuration exhibits a bell-shaped daily pattern that is beneficial for the load following strategy.

The same simulation output analysis was performed for the solar field configuration based on the solar tower with heliostat field. It has to be reminded that the optimization algorithm determined a lower aperture area for the CRS case. This leads to a lower solar input Q_{rad} to fulfill the heat demand, as documented in Fig. 13. Thanks to the 2-axis tracking system, the CRS exhibits a flat curve of the collected heat, with a peak of around 600 MW both for the summer and winter day.

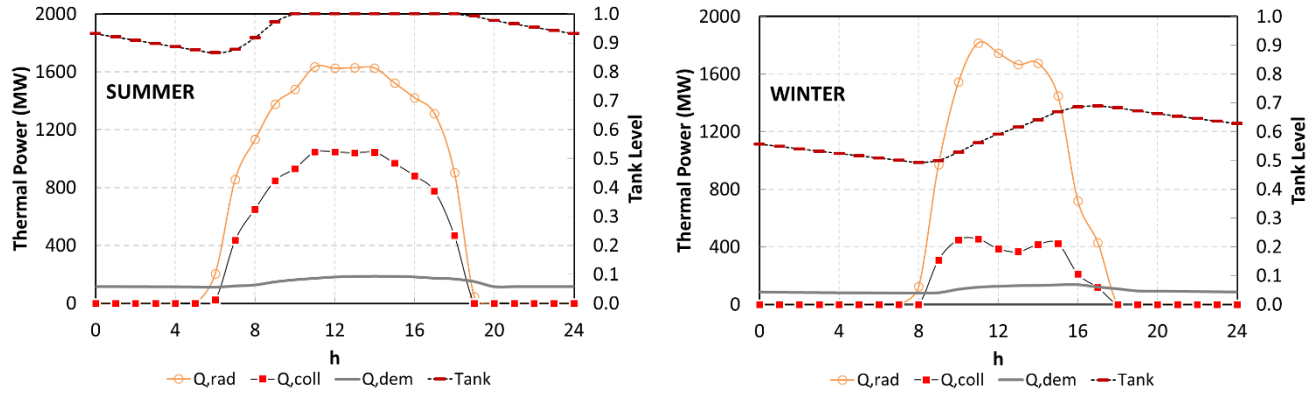

Fig. 11. Solar field daily simulation results (PTC configuration, north-south orientation).

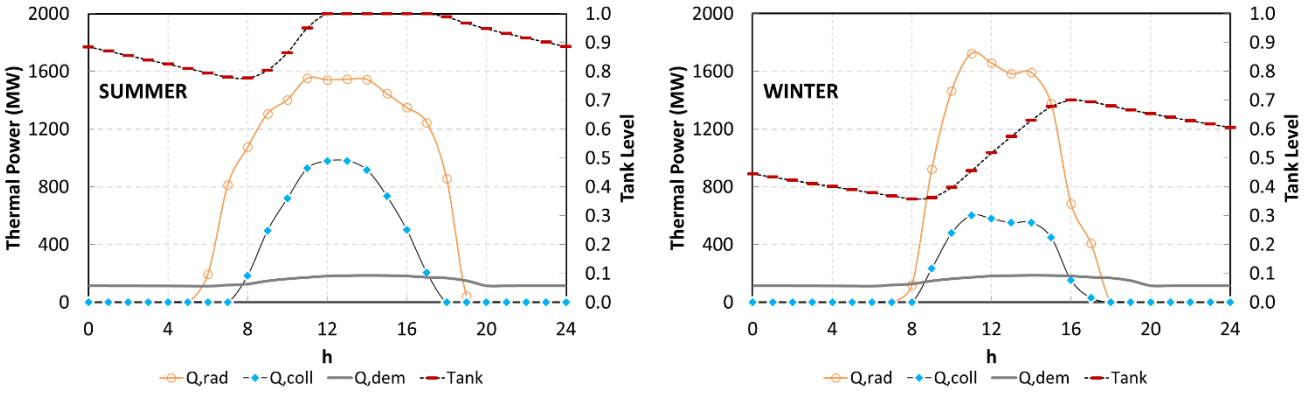

Fig. 12. Solar field daily simulation results (PTC configuration, east-west orientation).

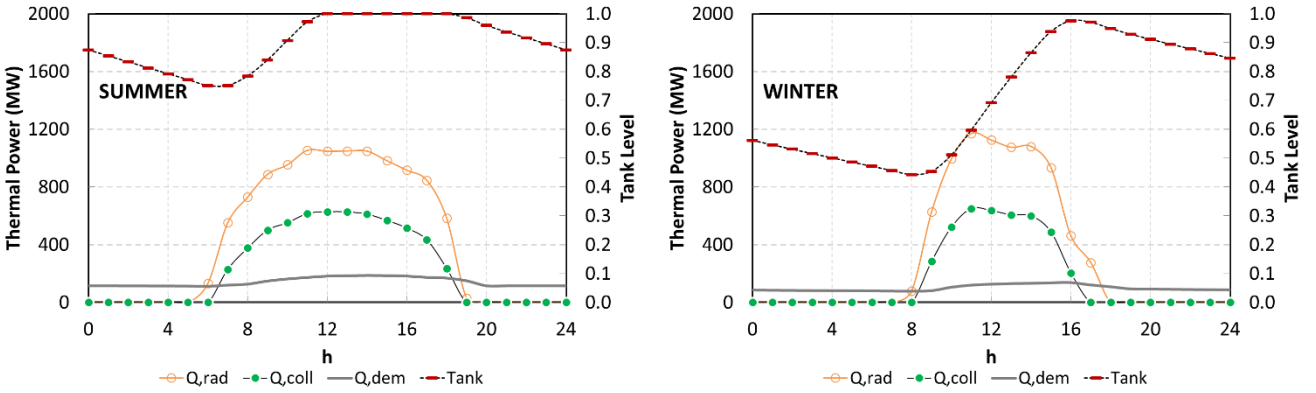

Fig. 13. Solar field daily simulation results (CRS configuration).

The behavior of the investigated solar fields is evaluated in more details in Fig. 14, where the solar-to-thermal efficiency is reported. In summer, parabolic troughs exhibit a very high efficiency (64%), whatever the axis orientation. East-west alignment has a penalty in efficiency in the early morning and late afternoon, when solar elevation is low. The efficiency of both north-south and east-west oriented PTC significantly decays in winter because of the cosine effect and lower ambient temperatures. The solar-to-thermal efficiency for CRS configuration is slightly lower in summer (59% vs. 64% in the central hours of the day),

ACCEPTED MANUSCRIPT

but significantly higher in winter (57% vs. 42%). This is due to the benefits of a 2-axis tracking system and to the reduced receiver area allowing for a minimization of thermal losses.

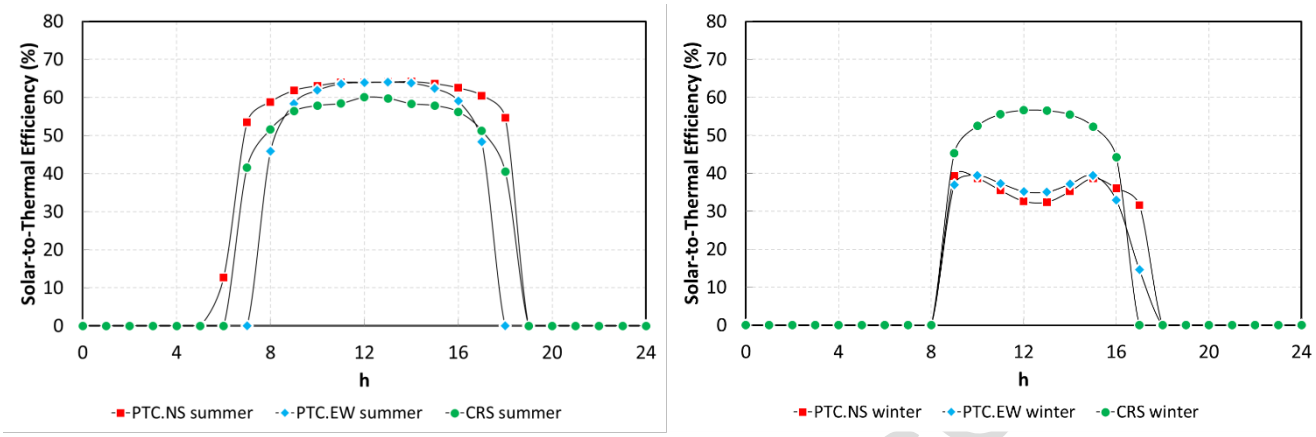

Fig. 14. Solar-to-Thermal Efficiency (%).

4.2. Monthly and yearly performance

Figs. 15-17 report on monthly basis the amount of the available solar energy (based on the DNI, E_{rad}), the heat potentially collected without defocusing (E_{coll}) and the actual collected heat corresponding to the power block thermal energy demand (E_{dem}), for the three CSP solutions. Different results were found depending on the solar field.

North-south oriented parabolic troughs (see Fig. 15) exhibit a relevant excess in the collected heat for a long period (from spring until late autumn) thus requiring the defocusing of several troughs (927 GWh annual overproduction). The large PTC aperture area responsible of the overproduction in the hottest months is necessary to meet the heat demand in winter when the trough efficiency is low. East-west oriented parabolic troughs (see Fig. 16) perform similarly in winter months, whilst they produce excess energy from March to October to a lesser extent than PTC with north-south orientation (423 GWh annual overproduction). An even better situation can be observed for solar tower configuration (Fig. 17); all over the year, even in summer months, CRS is capturing almost exactly the thermal energy (E_{dem}) required by the steam cycle, and only a moderate thermal dumping occurs in the hottest months (336 GWh annual overproduction). This behavior is strictly related to the heliostat field efficiency previously discussed.

ACCEPTED MANUSCRIPT

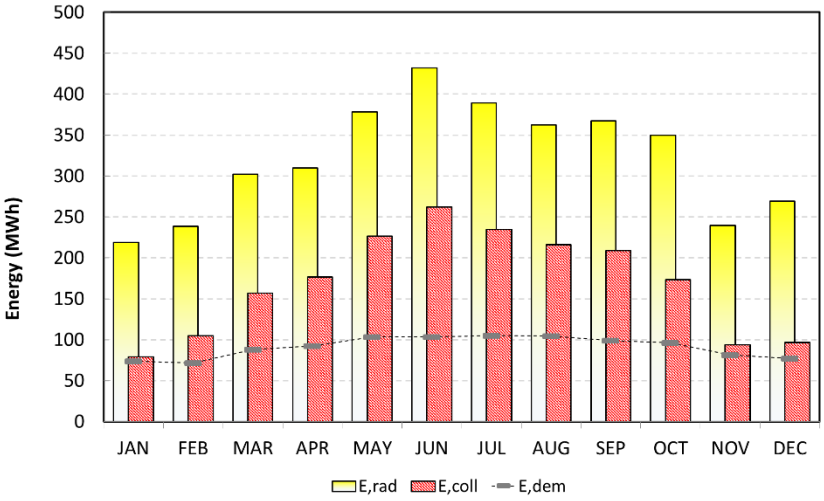

Fig. 15. Monthly results for north-south oriented PTCs.

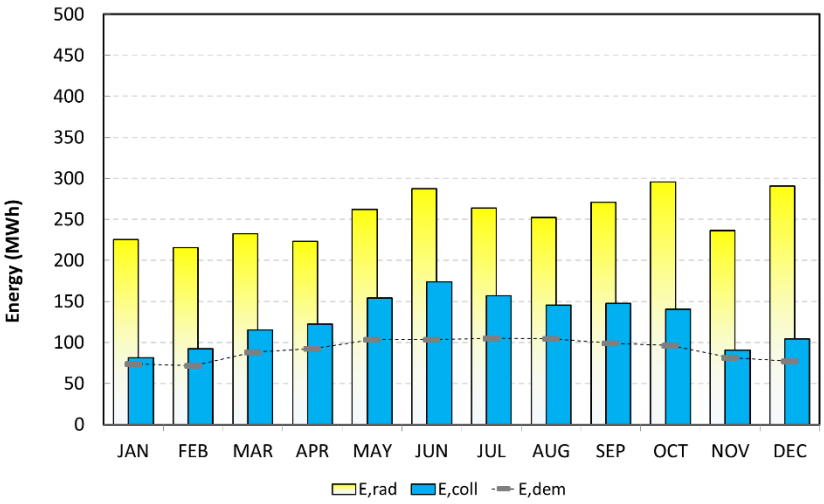

Fig. 16. Monthly results for east-west oriented PTCs.

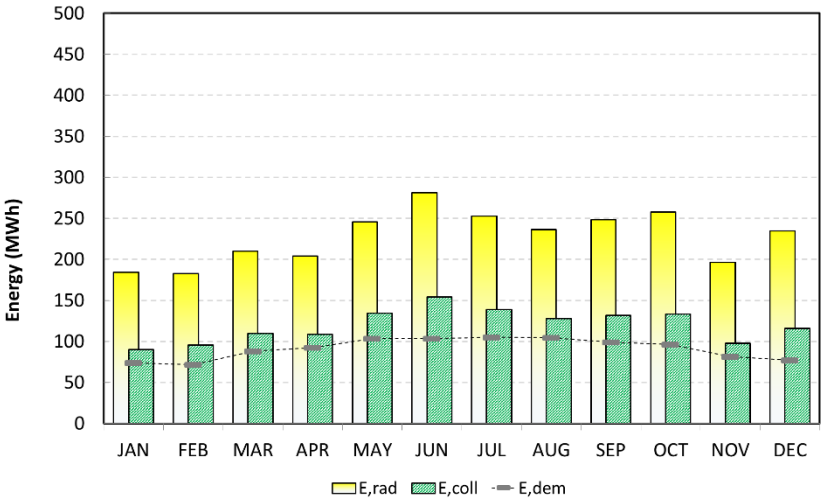

Fig. 17. Monthly results for CRS configuration.

ACCEPTED MANUSCRIPT

Table 6 reports the annual energy balance, which evaluates the overall performance of the investigated configurations. The heat demand is the same for all considered solar fields. To drive the power cycle, the CRS requires the lowest amount of solar energy on annual basis, and exhibits the minimum of unallocated surplus (23.4%). On the opposite, PTC with north-south orientation represents the worst case, with 45.7% annual overproduction since the collector field must be oversized to cover the heat demand in winter. The solution with east-west oriented PTCs takes advantage of a limited defocused energy (27.7% on annual basis) but suffers for the lowest average efficiency.

Table 6

PTC vs. CRS configurations: annual performance.

	$PTC_{north\text{-}south}$	$PTC_{east\text{-}west}$	CRS
Captured solar energy (GWh)	3857.4	3056.7	2734.1
Collected heat (GWh)	2029.7	1523.9	1436.8
Heat demand (GWh)	1090.7		
Energy surplus (%)	45.7%	27.7%	23.4%
Average efficiency (%)	52.6%	49.9%	52.6%

5. Economic sensitivity analysis

In order to evaluate the impact of the costs per unit (reported in Table 4) on the simulation results, a sensitivity analysis has been carried out. The cost per unit area of solar field was varied in the range 175-300 USD/m^2 for PTCs, and 225-350 USD/m^2 for CRS, whilst the cost for TES (not dependent on the solar field technology) was kept constant (30 USD/kWh). The optimization algorithm was run and GenOpt® determined the optimal values for aperture area and storage tank volume, minimizing the total budget cost (C). Fig. 18 shows the results of the sensitivity analysis. Filled symbols are referred to the budget cost reported in Table 4, whilst hollow symbols are related to the range of costs per unit area mentioned before. All total budget costs are normalized to the base CRS cost, as reference. CRS appears to be the best performing configuration for a wide range of cost per unit area ratio, thanks to the lower aperture area required to meet the power and cooling demand. For the PTC cases, the higher is the cost of solar field, the higher is the benefit of the east-west orientation for the considered load profile.

The charts in Fig. 19 report the variation of the optimal values for aperture area and tank volume, respectively. When the cost of solar field increases, the optimization algorithm finds out an optimum corresponding to a reduced aperture area and an increased storage volume for PTC cases. This trend is more remarkable for the east-west orientation. The optimum for CRS, on the contrary, appears substantially insensitive to the cost per unit area.

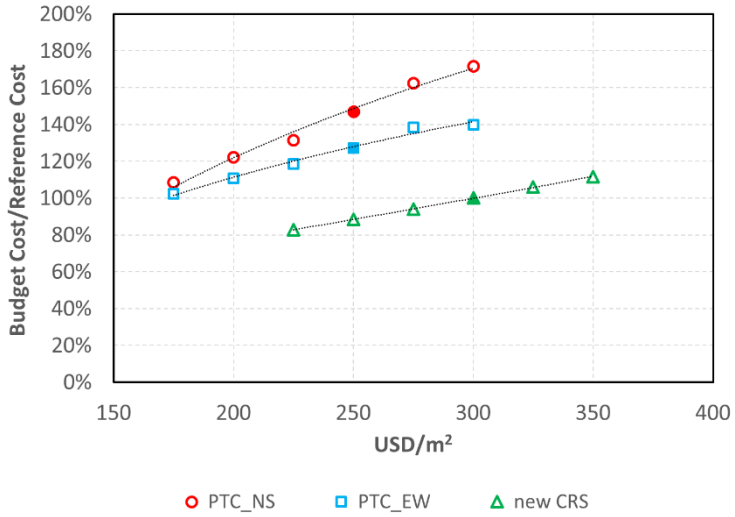

Fig. 18. Budget cost sensitivity analysis.

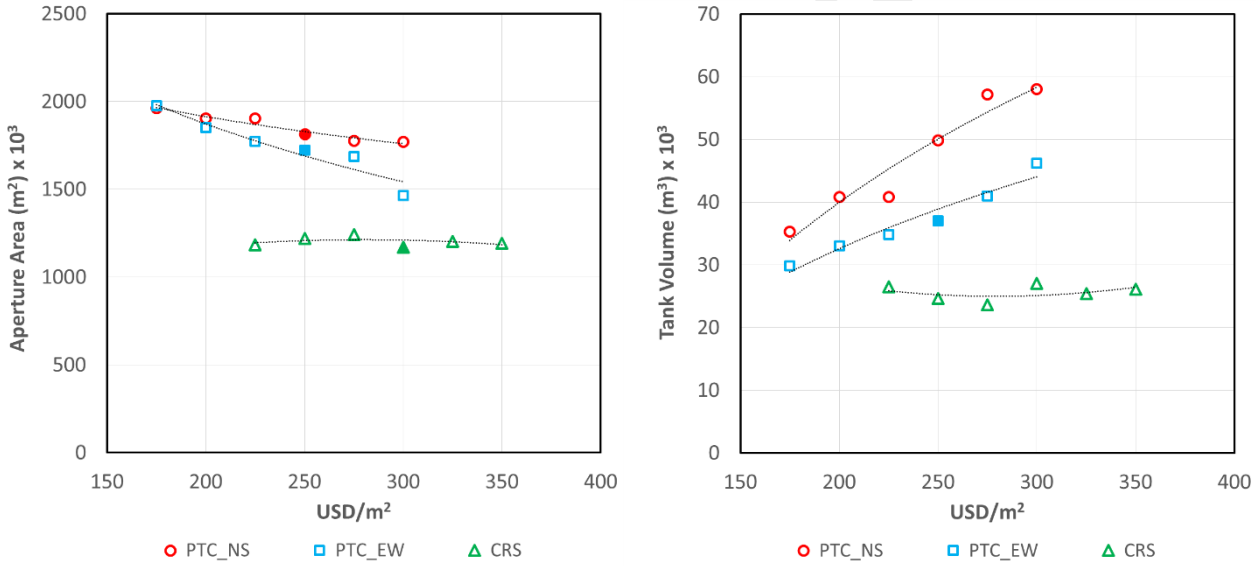

Fig. 19. Optimal values (solar field aperture area and tank volume).

6. Conclusions

The present work presented the simulation of a combined power and cooling plant driven by concentrated solar devices. The power block is based on a steam Rankine cycle, with steam extraction to feed double-effect absorption chillers. The CSP plant was designed to operate in "*island mode*" according with a load-following logic. Simulations were carried out for the climate conditions of a desert area in the Saudi region. Three different CSP technologies have been compared: north-south and east-west oriented PTCs, and CRS.

The beneficial effect of the combined power and cooling production has been documented for a CSP plant operating in island mode; the absorption chillers fed by low-grade steam allowed reducing significantly the power demand on the electrical grid, with a relevant peak shaving effect in summer. Concerning the solar field, for the resulting power demand PTC technology requires a larger aperture area than CRS to meet the Rankine cycle heat input. This is due to the combined power and cooling production, leading to a more flat

ACCEPTED MANUSCRIPT

energy demand that matches better the tower yield throughout the year. Therefore, the defocusing of some devices cannot be avoided in summer months but it can be reduced by choosing east-west oriented collectors instead of those aligned on a north-south axis. CRS provided the lowest thermal energy surplus and the collected heat slightly exceeds the power plant demand. The economic analysis showed that CRS is the solar field configuration allowing budget cost minimization, in spite of a higher cost per unit area; this is due to the reduced aperture area required to meet the power block heat demand. Simulation results showed that for a CSP plant operated with load-following strategy CRS is the best performing option.

References

[1] A. C. Köberle, D. E.H.J. Gernaat, D. P. van Vuuren, Assessing Current and Future Techno-economic Potential of Concentrated Solar Power and Photovoltaic Electricity Generation, Energy, 89, pp. 739-756, 2015.

[2] R. Guédez, J. Spelling, B. Laumert, Thermoeconomic Optimization of Solar Thermal Power Plants with Storage in High-Penetration Renewable Electricity Markets, Energy Procedia, 57, pp. 541-550, 2014.

[3] F. De Luca, V. Ferraro, V. Marinelli, On the Performance of CSP Oil-cooled plants, with and without Heat Storage in Tanks of Molten Salts, Energy, 83, pp. 230-239, 2015.

[4] Technology Roadmap, Concentrating Solar Power © OECD/IEA, 2010, International Energy Agency.

[5] A. Perdichizzi, G. Barigozzi, G. Franchini, S. Ravelli, Peak Shaving Strategy through a Solar Combined Cooling and Power System in Remote Hot Climate Areas, Applied Energy, 143, pp. 154-163, 2015.

[6] F.A. Boyaghchi, P. Heidarnejad, Thermoeconomic Assessment and Multi Objective Optimization of a Solar Micro CCHP based on Organic Rankine Cycle for Domestic Application, Energy Conversion and Management, 97, pp. 224-234, 2015.

[7] N. Petchers, Combined Heating, Cooling & Power Handbook: Technologies & Applications_An Integrated Approach to Energy Resource Optimization, The Fairmont Press, Inc., 2003.

[8] S. Sanaye, H. Hajabdollahi, Thermo-Economic Optimization of Solar CCHP Using Both Genetic and Particle Swarm Algorithms, Journal of Solar Energy Engineering, 137(1), 01101, 2014.

[9] P. Palenzuela, D.C. Alarcon-Padilla, G. Zaragozza, Large-Scale Solar Desalination by Combination with CSP: Techno-Economic Analysis of Different Options for the Mediterranean Sea and the Arabian Gulf, Desalination, 366, pp. 130-138, 2015.

[10] B. Ortega-Delgado, M. Cornali, P. Palenzuela, D.C. Alarcon-Padilla, Operational Analysis of the Coupling Between a Multi-Effect Distillation Unit with Thermal Vapor COmpression and a Rankine Cycle Power Block Using Variable Nozzle Thermocompressors, Applied Energy, 204, 690-701, 2017.

[11] Sargent, Lundy LLC Consulting Group, 2003. Assessment of Parabolic Trough and Power Tower Solar Technology Cost and Performance Forecasts. Subcontractor Report NREL/SR-550-34440, Chicago, USA.

[12] "Concentrating Solar Power Projects", https://www.nrel.gov/csp/solarpaces/index.cfm.

[13] U. Herrmann, B. Kelly, H. Price, Two-tank Molten Salt Storage for Parabolic Trough Solar Power Plants, Energy, 29, pp. 883-893, 2004.

ACCEPTED MANUSCRIPT

[14] H.L. Zhang, J. Baeyens, J. Degrève, G. Caceres, Concentrated Solar Power Plants: Review and Design Methodology, Renewable and Sustainable Energy Reviews, 22, pp. 466-481, 2013.

[15] G. Franchini, A. Perdichizzi, S. Ravelli, G. Barigozzi, A Comparative Study between Parabolic Trough and Solar Tower Technologies in Solar Rankine Cycle and Integrated Solar Combined Cycle Plants, Solar Energy, 98, pp. 302-314, 2013.

[16] S. Izquierdo, C. Montañes, C. Dopazo, N. Fueyo, Analysis of CSP Plants for the Definition of Energy Policies: the Influence on Electricity Cost of Solar Multiples, Capacity Factors and Energy Storage, Energy Policy, 38, pp. 6215-6221, 2010.

[17] E. Zarza, Medium Temperature Solar Concentrators (Parabolic-Troughs Collectors), Solar energy conversion and photoenergy systems, vol. 1, Eolss Publishers, 2009.

[18] D. Y. Goswami, F. Kreith, Energy conversion, CRC Press, 2008.

[19] K. Lovegrove, W. Stein, Concentrating Solar Power Technology: Principles, Developments and Applications, Woodhead Publishing Limited, 2012.

[20] A. Perdichizzi, G. Barigozzi, G. Franchini, S. Ravelli, Performance Prediction of a CSP Plant Integrated with Cooling Production, Energy Procedia, 75, pp. 436-443, 2015.

[21] F. Lippke (1995). Simulation of the Part-Load Behavior of a 30 MWe SEGS Plant. Sandia National Labs. Report SAND--95-1293.

[22] D. Kearney, U. Herrmann, P. Nava et al, Assessment of Molten Salt Heat Transfer Fluid in a Parabolic Trough Solar Field, J Solar Energy Eng-Trans ASME vol. 125, pp. 170-176, 2003.

[23] T. Moss, D. Brosseau, Testing capabilities NSTTF (AZTRAK) rotating platform. Sandia National laboratories, New Mexico, 2007.

[24] P. Garcia, A. Ferriere, J.-J. Bezian, Codes for Solar Flux Calculation Dedicated to Central Receiver System Applications: a Comparative Review, Solar Energy, 82, pp. 189-197, 2008.

[25] S. M. Besarati, D. Y. Goswami, E. K. Stefanakos, Optimal Heliostat Aiming Strategy for Uniform Distribution of Heat Flux on the Receiver of a Solar Power Tower Plant, Energy Conversion and Management, 84, pp. 234-243, 2014.

[26] N. Blair, A. Dobos, J. Freeman, T. Neises, M. Wagner, T. Ferguson, P. Gilman, S. Janzou, System Advisor Model, SAM 2014.1.14 – General Description, Nat. Renew. Energy Lab, Denver, CO, USA, Tech. Rep. NREL/TP-6A20-61019, February 2014.

[27] M. Wetter, "GenOpt-A Generic Optimization Program", proc. IBPSA's Building Simulation Conference, Rio de Janeiro, Brazil, August 2001.

[28] "CSP Today Global Tracker September 2016", http://social.csptoday.com/tracker/projects

[29] R. Pitz-Paal, J. Dersch, B. Milow, F. Téllez, et al., Development Steps for Parabolic Trough Solar Power Technologies with Maximum Impact on Cost Reduction, ASME Journal of Solar Energy Engineering, Vol. 129, No. 4, pp. 371-377, 2007.

Figure captions

Fig. 1. Electric load (P_{dem}) and chiller power consumption (P_{chill}).

Fig. 2. Schematic of the investigated CSP plant.

ACCEPTED MANUSCRIPT

ACCEPTED MANUSCRIPT

ACCEPTED MANUSCRIPT

Highlights

- A solar driven Rankine cycle, with cooling production, was simulated in island mode.
- Parabolic troughs and heliostat field with central receiver were assessed.
- North-south aligned parabolic troughs required the largest aperture area.
- Heliostats, with the lowest aperture area, provided the lowest thermal energy surplus.
- Heliostats with central receiver are the best solution in load-following operation.

ACCEPTED MANUSCRIPT